

# Geometry of transient chaos in streamwise-localized pipe flow turbulence

Nazmi Burak Budanur,<sup>1</sup> Akshunna Shaurya Dogra,<sup>2</sup> and Björn Hof<sup>1</sup>

<sup>1</sup>*Nonlinear Dynamics and Turbulence Group, IST Austria, 3400 Klosterneuburg, Austria*

<sup>2</sup>*Department of Physics, New York University, 726 Broadway, New York, NY 10003*

(Dated: November 8, 2021)

In pipes and channels, the onset of turbulence is initially dominated by localized transients, which lead to sustained turbulence through their collective dynamics. In the present work, we study the localized turbulence in pipe flow numerically and elucidate a state space structure that gives rise to transient chaos. Starting from the basin boundary separating laminar and turbulent flow, we identify transverse homoclinic orbits, the presence of which necessitates a homoclinic tangle and chaos. A direct consequence of the homoclinic tangle is the fractal nature of the laminar-turbulent boundary, which was conjectured in various earlier studies. By mapping the transverse intersections between the stable and unstable manifold of a periodic orbit, we identify the gateways that promote an escape from turbulence.

PACS numbers: 02.20.-a, 05.45.-a, 05.45.Jn, 47.27.ed

In wall-bounded shear flows close to onset, turbulence can be observed as localized patches that coexist with the orderly laminar flow that is stable against infinitesimal disturbances. In the case of pipe flow, these localized structures are known as puffs and they have a simple phenomenology: After a chaotic time-evolution, a puff might suddenly decay and disappear or split and give rise to a new puff. As the governing parameter, the Reynolds number ( $Re$ ), is increased, the mean puff lifetime before decaying increases while that before a splitting event decreases. This phenomenology was recently exploited to conceptualize a spatiotemporal description of the transition [1, 2]: In an infinitely long pipe that is initially populated with many puffs, turbulence will be sustained if the rate of puff splitting exceeds that of decay. Consequently, a critical  $Re_C$  is defined as the  $Re$ , at which both rates are equal.

In addition to allowing for a clear definition of the critical  $Re_C$ , the spatiotemporal dynamics also revealed universal properties of the transition to turbulence: critical exponents were determined in laboratory experiments for Couette flow [3] and in direct numerical simulations for Couette [3] and Waleffe flow, [4] and these suggest that the transition falls into the universality class of directed percolation.

Key to the above scenario is the existence of spatially independent chaotic transients. While the transient chaotic nature of the puff dynamics is evident from observations, how such dynamics arise from the Navier-Stokes equations is not well understood. Even though localized asymptotic states [5] and invariant solutions [6, 7] at the laminar-turbulent boundary were computed, dynamical routes for sudden puff decay across the stable manifold of such solutions were not identified. In this paper, we demonstrate the existence of homoclinic orbits in the vicinity of a periodic solution, which itself is on the laminar-turbulent boundary. Based on this observation, we suggest a global picture of the state space, containing a Smale horseshoe, which gives rise to transient chaos with a fractal basin boundary and thus, infinitely many paths for puff decay.

We simulate the incompressible fluid flow through a circular pipe of diameter  $D$  and length  $L = \pi D/0.1256637 \approx 25D$ . For this purpose, we employ `Openpipeflow` [8], which integrates the perturbations  $\mathbf{u}(z, r, \theta; t)$  to the base (Hagen-Poiseuille) solution  $\mathbf{u}_{HP}(z, r, \theta; t) = 2U(1 - (2r/D)^2)\hat{\mathbf{z}}$  of the pipe flow under periodic boundary condition  $\mathbf{u}(z, r, \theta; t) = \mathbf{u}(z + L, r, \theta; t)$  in the axial direction and no-slip boundary condition  $\mathbf{u}(z, r = D/2, \theta; t) = 0$  at the pipe wall. The Reynolds number is defined as  $Re = UD/\nu$ , where  $\nu$  is the kinematic viscosity of the fluid. In our simulations,  $Re = 1600$  and a constant flux is ensured via a time-varying axial pressure gradient. For the numerical representation, the flow fields are expanded in Fourier series truncated at  $K = 255$  and  $M = 47$  respectively in axial and azimuthal directions and with 64 finite-difference points were used in the radial direction. The nonlinear terms are evaluated following the 3/2-rule for dealiasing, leading to  $(768 \times 144 \times 64)$  grid points in the physical space. Time-stepping is performed by a second-order predictor-corrector method with a time-step  $\delta t \approx 0.00206D/U$ . The adequacy of this resolution is confirmed in the previous studies [6, 9], which examined similar parameter regimes using `Openpipeflow` with slightly lower resolutions. For the homoclinic orbits we are going to report in the following, the exponential drop-off of the Fourier coefficients is 4 orders of magnitude or more at every point along the orbit.

As in the ref. [7], the solutions that we consider are invariant under the reflection symmetry and azimuthal rotation by  $\pi$ ; i.e. the flow fields satisfy  $[u, v, w](z, r, \theta; t) = [u, v, -w](z, r, -\theta; t)$  and  $[u, v, w](z, r, \theta; t) = [u, v, w](z, r, \theta + \pi; t)$ , where  $u, v$ , and  $w$  respectively denote the  $z, r$ , and  $\theta$  components of the velocity field. After these restrictions, the remaining symmetries of pipe flow are the streamwise translations  $g_z(l)\mathbf{u}(z, r, \theta) = \mathbf{u}(z - l, r, \theta)$  and the azimuthal rotation by  $\pi/2$ :  $g_\theta(\pi/2)\mathbf{u}(z, r, \theta) = \mathbf{u}(z, r, \theta - \pi/2)$ . Here, we are going to reduce the translation symmetry via the first Fourier mode slice method [10] following its adaptation to the pipe flow in ref. [9]: Let  $\hat{u}_i = J_0(\alpha r) \cos(2\pi z/L)$ , where  $J_0$  is the Bessel function of the first kind,  $\alpha$  is chosen such that  $J_0(\alpha 2r/D) = 0$ , and  $i = 1, 2, 3$ . Then the symmetry-reduced velocity fields are given by  $\hat{\mathbf{u}}(t) = g_z(L\phi/2\pi)\mathbf{u}(t)$ , where  $\phi(t) = \arg(\langle \mathbf{u}(t), \hat{\mathbf{u}} \rangle + i \langle \mathbf{u}(t), g_z(-L/4)\hat{\mathbf{u}} \rangle)$  and  $\langle \cdot, \cdot \rangle$  denotes the  $L_2$  inner-product. See ref. [9] for details. In the remainder of this paper we use the symmetry-reduced description and drop the  $\hat{\cdot}$  signs.

Avila *et al.* [7] showed that in the above-described symmetry-invariant subspace, the laminar-turbulent boundary is set by the stable manifold of a relative periodic orbit, which is a periodic orbit with a streamwise shift. This orbit, which from here on we are going to refer to as LB, belongs to the lower branch of a pair of orbits that appear in a saddle-node bifurcation at  $Re \approx 1450$  in our domain [11]. After the symmetry-reduction, LB becomes a periodic orbit, which satisfies  $\mathbf{u}_{LB} = f^T(\mathbf{u}_{LB})$ , where  $f^t(\mathbf{u}(\mathbf{0})) = \mathbf{u}(t)$  denotes the finite-time flow mapping induced by the time-evolution under the Navier-Stokes equations and the symmetry-reduction,  $T$  is the period of LB, and  $\mathbf{u}_{LB}$  is an arbitrary point on the LB. Numerically, we converge to this solution up to a relative error of  $10^{-9}$  through Newton-GMRES-hookstep iterations [12] at  $Re = 1600$  using 6000 equally spaced time-steps along the orbit. We found LB's period at this  $Re$  to be  $T \approx 12.35 D/U$  and in the subsequent computations we used a fixed time-step  $\delta t = T/6000$  [13].

In order to study the linear stability and the unstable manifold of the LB, we define the Poincaré section as the set of velocity fields  $\tilde{\mathbf{u}}$  that satisfy

$$\langle \tilde{\mathbf{u}} - \tilde{\mathbf{u}}_{LB}, \partial_t \tilde{\mathbf{u}}_{LB} \rangle = 0 \text{ and } \langle \partial_t \tilde{\mathbf{u}}, \partial_t \tilde{\mathbf{u}}_{LB} \rangle > 0, \quad (1)$$

where  $\tilde{\mathbf{u}}_{LB}$  is an arbitrarily-chosen point on the LB. Numerically, we approximated  $\partial_t \mathbf{u}$  as the first-order finite difference  $\partial_t \mathbf{u} \approx (f^{\delta t}(\mathbf{u}) - \mathbf{u})/\delta t$ , since its accuracy does not affect the accuracy of the steps that follow. Geometrically,

(1) describes a half-hyperplane in the infinite-dimensional state space that accommodates the solutions to the Navier–Stokes equations. This construction, along with the evolution under the Navier–Stokes equations, implies a discrete-time dynamical system, i.e. the Poincaré map

$$\tilde{\mathbf{u}}[n+1] = \mathcal{P}(\tilde{\mathbf{u}}[n]) = f^{\Delta t_n}(\tilde{\mathbf{u}}[n]), \quad (2)$$

where  $n$  is the discrete-time variable and  $\Delta t_n$  is the first return time, which is the minimum time that is necessary for the state space trajectory to intersect the Poincaré section (1) after leaving it. In order to find  $\Delta t_n$  in simulations, we first integrate a trajectory with our fixed time-step  $\delta t$  and identify consecutive states for which the hyperplane condition in (1) changes its sign from  $-$  to  $+$ . We then carry out a bisection search in time-steps until the hyperplane condition is satisfied with a relative error of  $10^{-9}$ .

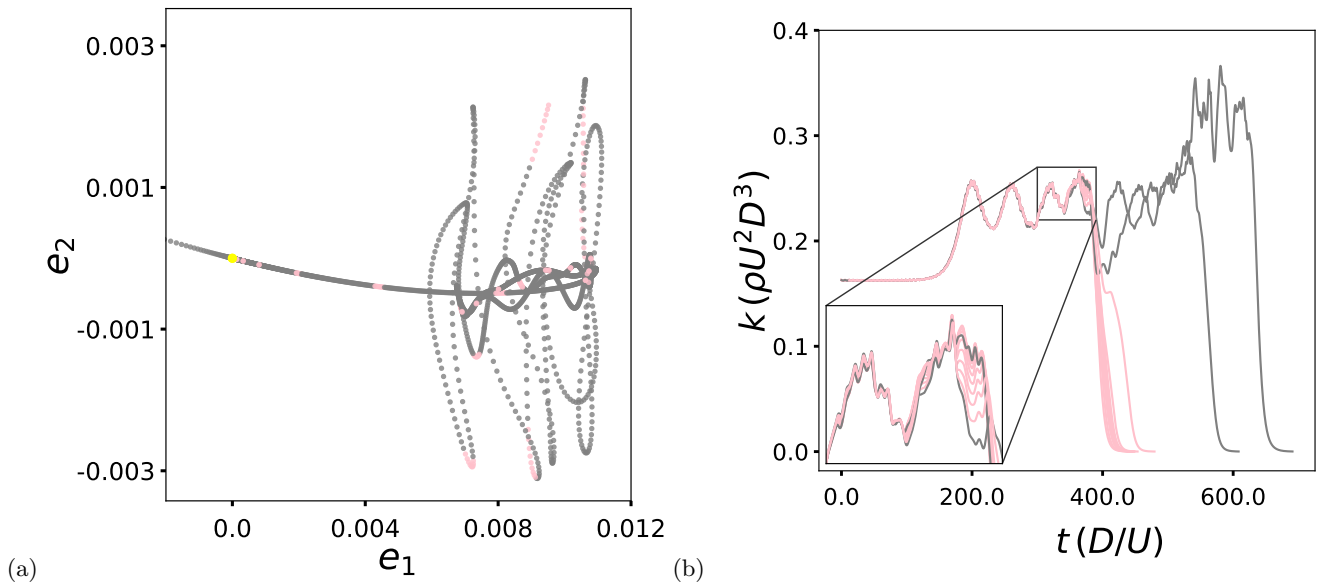


FIG. 1. (a) (color online) Two-dimensional projection of unstable manifold of LB computed within the Poincaré section (1) by forward integrating initial points (4). Nearby trajectories that laminarize around the same time are colored pink. (b) Time-series of the kinetic energy for the initial conditions (4) with  $\delta \in [0.0, 0.08]$  and  $\delta \in [0.97, 0.99]$ . The latter shifted by  $T$  in time to better illustrate the similarity of the time-series.  $\delta = 0.08$  and  $\delta = 0.97$  are shown gray, and the rest, which laminarize around the same time, are shown pink.

By construction,  $\tilde{\mathbf{u}}_{LB}$  is a fixed point of the Poincaré map. Linear stability of  $\tilde{\mathbf{u}}_{LB}$  is then described by the eigenvalue problem

$$[D\mathcal{P}(\tilde{\mathbf{u}}_{LB})] \tilde{V}_i = \Lambda_i \tilde{V}_i, \quad (3)$$

where  $[D\mathcal{P}(\cdot)]$  is the Jacobian of the Poincaré map and  $\Lambda_i, \tilde{V}_i$  respectively are the stability eigenvalues and eigenvectors of  $\tilde{\mathbf{u}}_{LB}$ . We approximate the leading 5 stability eigenvalues and eigenvectors of the LB using Arnoldi iteration [14] such that  $\text{Re} \Lambda_1 \geq \text{Re} \Lambda_2 \geq \dots \geq \text{Re} \Lambda_5$ . We found that LB has one unstable direction with the associated eigenvalue  $\Lambda_1 \approx 2.52$  and its leading stable eigenvalue to be  $\Lambda_{2,3} \approx 0.638 \pm i0.409$ .

In order to approximate the LB's unstable manifold, we iterate the Poincaré map (2) starting with the initial conditions

$$\tilde{\mathbf{u}}(\delta) = \tilde{\mathbf{u}}_{LB} \pm \epsilon \Lambda_1^\delta \tilde{V}_1, \quad (4)$$

where  $\epsilon = 10^{-6}$  is a small constant,  $\delta \in [0, 1)$  is a cyclic ( $\tilde{\mathbf{u}}(1) \approx \mathcal{P}(\tilde{\mathbf{u}}(0))$ ) variable that parametrizes the manifold along with the discrete time  $n$ , and  $\tilde{V}_1$  is normalized such that  $\|\tilde{V}_1\| = \|\tilde{\mathbf{u}}_{LB}\|$  in  $L_2$  (energy) norm. We approximated the unstable manifold of the LB by iterating the initial conditions (4) using 10 and 100 equally spaced points for  $\delta$  respectively in the  $-\tilde{V}_1$  and  $+\tilde{V}_1$  directions. We visualized this manifold as a projection onto  $\tilde{V}_1$  and  $\text{Re} \tilde{V}_2$  in figure 1 (a), where the origin is located at  $\tilde{\mathbf{u}}_{LB}$ . Explicitly, the projections are obtained as  $e_1 = \langle \tilde{\mathbf{u}} - \tilde{\mathbf{u}}_{LB}, \tilde{V}_1 \rangle$  and  $e_2 = \langle \tilde{\mathbf{u}} - \tilde{\mathbf{u}}_{LB}, \text{Re} \tilde{V}_2 \rangle$ .

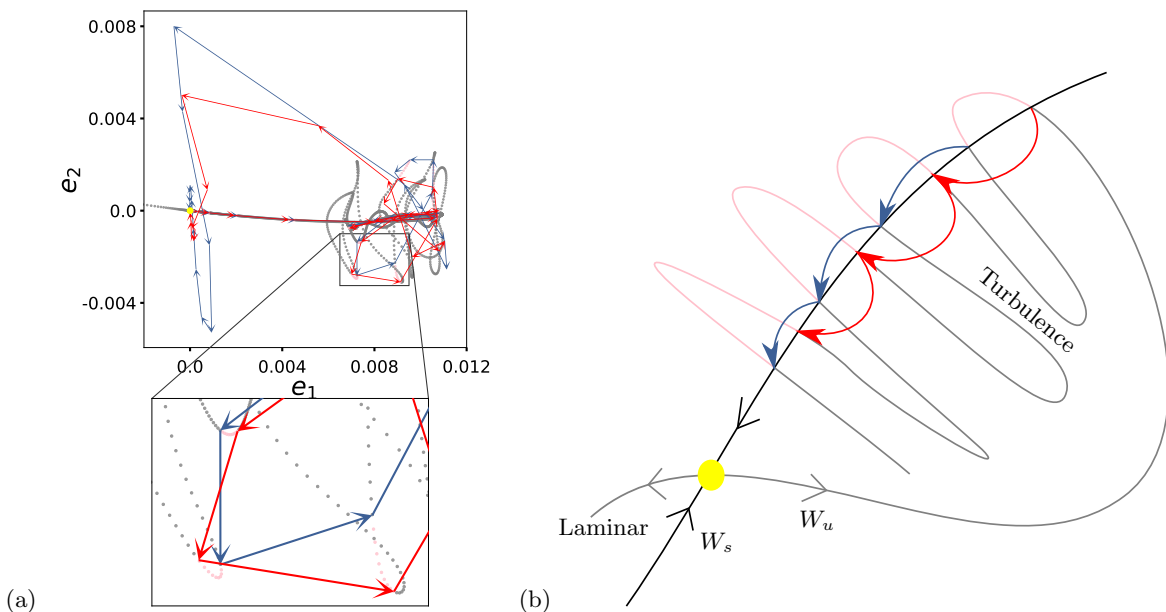


FIG. 2. (color online) (a) The approximations to the homoclinic orbits (blue and red) and the unstable manifold of the LB. Arrows show the direction of time. Inset zooms in to the indicated region in order to better visualize that the homoclinic orbits lie inbetween the orbits that laminarize together and those that further explore turbulent parts of the state space. (b) A “cartoon” of the state space based on the results shown in (a).  $W_s$  and  $W_u$  respectively denote stable and unstable manifolds; the laminarizing trajectories and the homoclinic orbits use the same color scheme as in (a).

In figure 1(a), we have shown few points in  $-\tilde{V}_1$  since all of these points uneventfully laminarize[15]. The trajectories, which are initiated in the  $+\tilde{V}_1$  direction, on the other hand, explore the chaotic regions of the state space before eventually laminarizing. We observed that the trajectories of the initial conditions (4) with  $\delta = 0.0, 0.01, \dots, 0.07$  and  $\delta = 0.98, 0.99$ , which are colored pink in figure 1, laminarize around the same time when the time-series for  $\delta = 0.98$  and  $0.99$  is shifted by one-period  $T$ ; see figure 1(b). This observation suggests that these orbits cross the laminar-turbulent boundary, which is set by the stable manifold of the LB, in the same region of the state space. Thus, we expect to find *homoclinic orbits* that lie at the transverse intersections of the LB’s stable and unstable manifolds within the intervals  $\delta \in (0.07, 0.08)$  and  $\delta \in (0.97, 0.98)$ . In order to test this hypothesis, we bisect between the trajectories that laminarize after  $t = 400D/U$  and those that further visit the turbulent parts of the state space in both  $\delta$ -intervals. This procedure indeed yields orbits that come back to the LB as can be seen on figure 2 (a), where we projected these orbits on top of the unstable manifold of figure 1(a). The projection coordinates are same in both figures.

When the bisections are carried out up to the numerical precision, our approximations to the homoclinic orbits come as close as  $\|\tilde{u}_{hc} - \tilde{u}_{LB}\|/\|\tilde{u}_{LB}\| \sim 10^{-3}$  to the LB. Further evidence can be seen from the flow structure visualizations of figure 3, where the initial and final snapshots of homoclinic orbits are virtually indistinguishable.

The presence of a transverse homoclinic point has profound consequences:

(i) Every forward or backward iteration of a homoclinic point is another crossing of the stable and unstable manifolds, hence, when the stable and unstable manifolds intersect at one point, they do so at infinitely many points as sketched in figure 2 (b).

(ii) Transverse intersection of the stable and unstable manifolds implies a *horseshoe* [16], which necessitates a countable infinity of periodic and an uncountable infinity of aperiodic orbits; hence chaos.

(iii) In the particular case we consider here, the stable manifold of the solution is the boundary of the laminar equilibrium’s domain of attraction, thus, infinitely many intersections of the stable and unstable manifolds yield infinitely many dynamical routes to puff decay.

These three points together imply *transient chaos* [17], which is the central assumption of the experiments that study the transition to turbulence through a spatiotemporal intermittency [1–3].

Van Veen and Kawahara [18] computed homoclinic orbits from the edge of chaos in a small computational cell of the plane Couette flow at  $Re = 400$  [19]. At this regime, plane Couette flow can be transient in small computational cells, however, it is sustained in large-enough domains [20]. Hence they highlighted the resemblance of the homoclinic orbits to the so-called turbulent bursting event. Here, we argue that the presence of the homoclinic structure necessitates

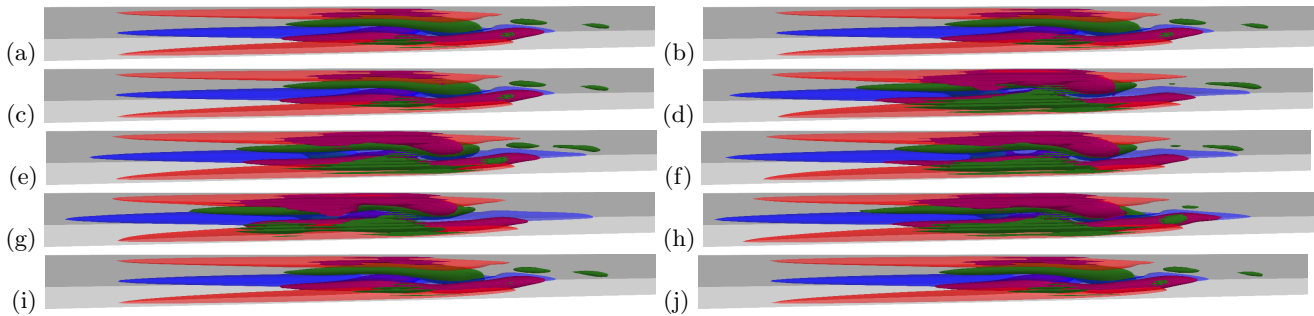


FIG. 3. (color online) Isosurfaces of the streamwise velocity fluctuations at  $\pm 0.3U$  (red-blue) and the streamwise vorticity at  $\pm 0.8U/D$  (purple-green) visualized for a homoclinic orbit on the Poincaré section at times  $n = 0, 5, 10, 15, 20, 25, 30, 35, 40, 45$  ( $t = 0.0, \dots, 486.95$ ) (a–j). A quarter ( $\theta \in [0, \pi/2)$ ) of the domain is shown since the rest can be obtained from the symmetries. Similar visualization of  $\tilde{\mathbf{u}}_{LB}$  is indistinguishable from (a), hence not shown separately.

transient chaos and thus, provides an explanation of how turbulent puffs can cross the laminar-turbulent boundary and then rapidly decay to laminar flow.

The symmetry-invariant subspace we studied in this paper carries the main features of the pipe flow, however, one should keep in mind that the complete physics of the pipe flow is richer than what we have considered here. We already know that there exists a relative periodic orbit with a threefold azimuthal symmetry [6] analogous to the one we studied here, and it is conceivable that there exists other relative periodic orbits at the laminar-turbulent boundary. We speculate that other such relative periodic orbits would also have unstable manifolds that contain homoclinic orbits, yielding the full complexity of the localized turbulence in pipe flow.

The existence of fractal basin boundaries in transitional shear flows was previously suggested in the light of numerical experiments [21–23]. Our results here clearly show that this must indeed be the case for the streamwise-localized turbulence in pipe flow as a consequence of the homoclinic tangle [24].

At the first stage of our investigation, we identified a set of trajectories that belong to a continuum of trajectories that leave the turbulent part of the state space. While not at the focus of the current work, we would like to remark that this methodology might be exploited for control purposes. In order to eliminate turbulence in a transitional setting like ours, the flow must be driven towards the laminarizing side of the edge state’s stable manifold. However, there exists no method for approximating this manifold since the time-backward integration is not possible. Therefore, locating parts of the unstable manifold that intersect the stable manifold could be a starting point for perturbing the system in this direction.

We confirmed the existence of homoclinic orbits at higher resolutions by partially repeating our computations with  $(K, M, N) = (383, 47, 96)$  and half of the time-step. We would like to note that increasing the resolution changes the appearance of the computed manifold and precise location of homoclinic orbits. We believe that these variations are due to the differences in the flow regime upon changing the resolution. Avila *et al.* [7] already reported that the changes in resolution shifted the bifurcation points while leaving the qualitative scenario unchanged and we think that our situation here is similar. Our result, along with the recent paper by Lustro *et al.* [25], who followed a very similar methodology to elucidate the homoclinic tangency in a minimal plane Couette flow, suggest numerical methods for computing homoclinic orbits in high-dimensional systems as an important technical challenge.

In summary, we have studied the unstable manifold of a streamwise-localized relative periodic orbit on the laminar-turbulent boundary of pipe flow and showed that it accommodates homoclinic orbits. We argue that this structure qualitatively explains the transient chaos that is observed in the computer and laboratory experiments of the spatially localized turbulence in pipe flow.

## ACKNOWLEDGMENTS

ASD acknowledges the financial support from OeAD Sonderstipendien, Österreichische Austauschdienst-Gesellschaft – Austria and Dean’s Undergraduate Research Fund Grant (DURF), College of Arts and Sciences (NYU). We are also grateful to the Scientific Computing Unit at IST Austria, which maintains the IST high performance computing

cluster, where all simulations presented in this paper were performed.

- 
- [1] K. Avila, D. Moxey, A. de Lozar, M. Avila, D. Barkley, and B. Hof, “The onset of turbulence in pipe flow,” *Science* **333**, 192–196 (2011).
  - [2] V. Mukund and B. Hof, “The critical point of the transition to turbulence in pipe flow,” *J. Fluid Mech.* **839**, 76–94 (2018).
  - [3] G. Lemoult, L. Shi, K. Avila, S. V. Jalikop, M. Avila, and B. Hof, “Directed percolation phase transition to sustained turbulence in Couette flow,” *Nat Phys* **12**, 254–258 (2016).
  - [4] M. Chantry, L. S. Tuckerman, and D. Barkley, “Universal continuous transition to turbulence in a planar shear flow,” *J. Fluid Mech.* **824**, R1 (2017).
  - [5] F. Mellibovsky, A. Meseguer, T. M. Schneider, and B. Eckhardt, “Transition in localized pipe flow turbulence,” *Phys. Rev. Lett.* **103**, 054502 (2009).
  - [6] M. Chantry, A. P. Willis, and R. R. Kerswell, “Genesis of streamwise-localized solutions from globally periodic traveling waves in pipe flow,” *Phys. Rev. Lett.* **112**, 164501 (2014).
  - [7] M. Avila, F. Mellibovsky, N. Roland, and B. Hof, “Streamwise-localized solutions at the onset of turbulence in pipe flow,” *Phys. Rev. Lett.* **110**, 224502 (2013).
  - [8] A. P. Willis, “The Openpipeflow Navier-Stokes solver,” *SoftwareX* **6**, 124 – 127 (2017).
  - [9] N. B. Budanur and B. Hof, “Heteroclinic path to spatially localized chaos in pipe flow,” *J. Fluid Mech.* **827**, R1 (2017), 10.1017/jfm.2017.516.
  - [10] N. B. Budanur, P. Cvitanović, R. L. Davidchack, and E. Siminos, “Reduction of the SO(2) symmetry for spatially extended dynamical systems,” *Phys. Rev. Lett.* **114**, 084102 (2015).
  - [11] The exact bifurcation point varies slightly depending on the domain length and the resolution.
  - [12] D. Viswanath, “Recurrent motions within plane Couette turbulence,” *J. Fluid Mech.* **580**, 339–358 (2007), [arXiv:physics/0604062](https://arxiv.org/abs/physics/0604062).
  - [13] This was necessary in order to compute the unstable manifold of LB accurately since the relative periodic orbit and its linear stability eigenvectors were converged with this time-step. We confirmed that this behavior is consistent by repeating parts of the computation with a time-step  $\delta t/2$ .
  - [14] L. N. Trefethen and D. Bau, *Numerical Linear Algebra* (SIAM, 1997).
  - [15] The sign, of course, is merely a convention.
  - [16] S. Smale, “Differentiable dynamical systems,” *Bull. Amer. Math. Soc.* **73**, 747–817 (1967).
  - [17] B. Hof, J. Westerweel, T. M. Schneider, and B. Eckhardt, “Finite lifetime of turbulence in shear flows,” *Nature* **443**, 59–62 (2006).
  - [18] L. van Veen and G. Kawahara, “Homoclinic tangle on the edge of shear turbulence,” *Phys. Rev. Lett.* **107**, 114501 (2011).
  - [19]  $Re$  based on half the velocity difference between the two walls and half the wall separation.
  - [20] Y. Duguet, P. Schlatter, and D. S. Henningson, “Formation of turbulent patterns near the onset of transition in plane couette flow,” *J. Fluid Mech.* **650**, 119–129 (2010).
  - [21] J. Moehlis, B. Eckhardt, and H. Faisst, “Fractal lifetimes in the transition to turbulence,” *Chaos* **14**, S11 (2004).
  - [22] P. Ritter, F. Mellibovsky, and M. Avila, “Emergence of spatio-temporal dynamics from exact coherent solutions in pipe flow,” *New J. Phys.* **18**, 083031 (2016).
  - [23] T. Kreilos, B. Eckhardt, and T. M. Schneider, “Increasing lifetimes and the growing saddles of shear flow turbulence,” *Phys. Rev. Lett.* **112**, 044503 (2014).
  - [24] S. W. McDonald, C. Grebogi, E. Ott, and J. A. Yorke, “Fractal basin boundaries,” *Physica D* **17**, 125–153 (1985).
  - [25] J. R. T. Lustro, G. Kawahara, L. van Veen, M. Shimizu, and H. Kokubu, “The onset of transient turbulence in minimal plane couette flow,” *J. Fluid Mech.* **862**, R2 (2019).